Biobased and Compostable Multiblock Copolymer of Poly(l-lactic acid) Containing 2,5-Furandicarboxylic Acid for Sustainable Food Packaging: The Role of Parent Homopolymers in the Composting Kinetics and Mechanism

(Article begins on next page)

19 October 2024

Biobased and compostable multiblock copolymer of poly(L-lactic acid) containing 2,5-furandicarboxylic acid for sustainable food packaging. The role of the parent homopolymers in the composting kinetics and mechanism

Enrico Bianchi[a†], Giulia Guidotti[a†], Michelina Soccio[a,e]*, Valentina Siracusa[b], Massimo Gazzano[c], Elisabetta Salatelli[d], Nadia Lotti[a,e,f]

[a]Civil, Chemical, Environmental and Materials Engineering Department, University of Bologna, Via Terracini 28, 40131 Bologna, Italy.

[b]Department of Chemical Science, University of Catania, Viale A. Doria 6, Catania 95125, Italy.

[c]Institute for Organic Synthesis and Photoreactivity, ISOF-CNR, Via Gobetti 101, 40129 Bologna, Italy.

[d]Department of Industrial Chemistry "Toso Montanari", University of Bologna, Viale Risorgimento 4, 40136 Bologna, Italy.

[e]Interdepartmental Center for Industrial Research on Advanced Applications in Mechanical Engineering and Materials Technology, CIRI-MAM, University of Bologna, Bologna, Italy.

[f]Interdepartmental Center for Agro-Food Research, CIRI-AGRO, University of Bologna, Bologna, Italy.

[†] These authors contributed equally

*Corresponding Author: Michelina Soccio m.soccio@unibo.it

Abstract

In the last years, the exponential growth in the demand of petroleum-based plastic materials, besides the extreme exploitation of non-renewable resources, lead to the mismanagement of their disposal and to serious ecological issues related to their dispersion in the environment. Among the possible practical solutions, the design of biobased and biodegradable polymers represents one of the most innovative challenges. In such a context, the eco-design of an aromatic-aliphatic multiblock copolymer based on poly(lactic acid) and containing 2,5-furandicarboxylic acid was carried out with the aim of improving the properties of poly(L-lactic acid) for sustainable packaging applications. The synthetic method followed a novel top-down approach, starting from industrial high-molecular-weight poly(L-lactic acid) (PLLA), which was reacted with 1,5-pentanediol to get hydroxyl-terminated PLLA and then chain-extended with hydroxyl-terminated poly(pentamethylene furanoate) (PPeF-OH). The final copolymer, called P(LLA50PeF50)-CE, was subjected to molecular, structural and thermal characterization. Tensile and gas permeability tests were also carried out. According to the results obtained, PLLA thermal stability was improved, being the range of processing temperatures widened, and its stiffness and brittleness were decreased, making the new material suitable for the realization of films for flexible packaging. The oxygen permeability of PLLA was decreased by 40% and a similar improvement was measured also for carbon dioxide. P(LLA50PeF50)-CE was found to be completely biodegraded within 60 days of composting treatment. In terms of mechanism, the blocks of PPeF and PLLA were demonstrated to undergo surface erosion and bulk hydrolysis, respectively. In terms of kinetics, PPeF blocks degraded slower than PLLA ones.

Keywords: 2,5-furandicarboxylic acid; poly(L-lactic acid); aromatic-aliphatic polyester; block copolymer; composting mechanism; sustainable packaging.

Introduction

Over the last century, plastics have offered innovative solutions to Society's permanently evolving needs and challenges. The exponential growth of their production has nonetheless led this class of materials to become a challenge in their own respect, particularly for the environmental issues caused by the still massive use of fossil sources and the mismanagement of plastics disposal. As a matter of fact, the production of polymeric materials in Europe amounted to 57.2 million tons in 2021 of which 39.1% was used for packaging applications[1]. Even though technological and societal advancements have been improving the efficiency of recycling systems, 6.9 million tons of post-consumer plastic waste were still destined to the landfill in 2020, of the 29.5 million tons collected in Europe[1]. Therefore, it is crucial to ensure that plastics continue to deliver benefits to our society while having a low impact on the environment. One of the most promising solutions to reach this goal is the development and production of biobased and biodegradable polymeric materials. Just as much as in the case of conventional plastics, packaging is a predominant market sector in the production of bioplastics too, covering 48% of the global production capacity of bioplastics in 2022[2]. This large amount is subdivided in 0.38 and 0.69 million tons of rigid and flexible packaging, respectively[2]. Overall, the production capacity of bioplastics has been increasing in recent years and globally amounted to 2.2 million tons in 2022[2], a considerable portion of which (20.7%) was comprised of poly(lactic acid) (PLA). The market share percentage of PLA is predicted to remain stable in the coming years, following the growth of the global demand of bioplastics, which is estimated to amount to 6.3 million tons by 2027[2]. PLA has been widely studied over the years as a promising biopolymer for special short-term applications, such as household items[3], food packaging[4–6], mulching films[7] and biomedical technologies[8,9], all of which benefit from the fast degradability and good biocompatibility of PLA. Since most life cycle assessment (LCA) studies confirm that the substitution of petrochemical plastics with biobased ones leads to a decrease in CO_2 emissions[10], it is worth stressing that PLA can be entirely produced from renewable resources: first- or second-generation biobased feedstocks (sugars or agricultural waste, respectively) can be fermented to obtain enantiomerically pure L-lactic acid, which can be turned into the corresponding lactide and finally into poly-L-lactic acid (PLLA) with a ring-opening polymerization. In spite of its industrial maturity, the potential uses of PLA are restricted by a number of limitations, such as low thermal stability, brittleness, hydrophobicity and moderate gas-barrier properties[11–13]. These limitations could be overcome in the perspective of: *1.* facilitating the use of PLLA for the manufacturing of flexible packaging, a field of application which was found through LCA studies to be distinctly more sustainable than the rigid one[14]; *2.* developing new polymeric materials for the production of monolayer flexible packaging, considerably easier to recycle than the state-of-the-art, commonly-used multilayer systems[15]. Furthermore, biodegradable

polymers such as PLLA are particularly suited for food-contact applications: indeed, the contamination of the material with biologic substances and the short shelf-life of foodstuffs pose a challenge for the recycling chain, making the disposal of non-recyclable food packaging in compost a more appealing option. Improving the barrier properties of PLLA would also enhance its performances in a key sector such as food packaging.

For all these reasons, the aim of this work was to selectively overcome the limitations of PLLA without compromising its compostability, with the use of a co-monomer, 2,5-furandicarboxylic acid (2,5-FDCA), which is one of the 12 most promising biobased building blocks on the market[16] and from which an entire class of aromatic polyesters can be obtained[17–19]. Other studies were able to achieve the modification of PLA with furan-based polyesters in the past, obtaining blends with poly(alkylene furanoate)s of various chain length[20–22], random copolymers with poly(ethylene furanoate)[23–25] and various kinds of block copolymers. Most notably, Guidotti et al. were able to prepare block copolyesters of poly(hexamethylene furanoate) (PHF)[26] or PLA[27] with PEG-like subunits via chain-extension, and Flores et al. could obtain a triblock copolymer of PLA and PHF by ring-opening polymerization (ROP)[28]. These multiblock systems are of particular interest for their ability to merge the valuable properties of both their homopolymers of reference. This observation, paired with the fact that aliphatic-aromatic polyesters such as PBAT showcase both excellent functional properties and noteworthy biodegradability[29], lead to an aromatic-aliphatic block copolymer as the molecular architecture of choice for the present study. Among furan-based polyesters, poly(pentamethylene furanoate) (PPeF), thanks to its outstanding functional properties especially for applications in the field of sustainable food packaging, was the reference homopolymer chosen to synthesize multiblock copolymer with PLLA. PPeF is not yet produced on an industrial scale, but it has been studied in recent years and its exceptional performances[30–34] were correlated with evidence of the formation of a 2D-ordered phase[35–37] in its otherwise amorphous structure. Specifically, PPeF was reported to have a mechanical behavior akin to a thermoplastic elastomer, with elongation at break higher than 1000 %, resistance to thermal degradation up to 392 °C and most importantly, gas barrier properties comparable to those of poly(vinyl alcohol), a commonly used gas-barrier layer in multilayer food packaging systems[38]. These properties have the potential of greatly improving the widely-available PLLA in its key limitations, as they were previously discussed. Moreover, evidence suggested that furan-based polyesters might be readily biodegradable in spite of their aromatic nature[39], implying that a copolymerization with PLLA would not result in inferior compostability.

The synthetic method designed for this work (Scheme 1) was innovative, not only because of the novelty of a block copolymerization reaction of PLLA with PPeF, but also because of the novelty of

the top-down copolymerization approach, aimed at improving high-molecular weight, industrially produced PLLA. Biobased reagents were used in a green, solvent-free process by which first, high-molecular weight PLLA was hydroxy-functionalized under controlled conditions and then, copolymerized with hydroxy-terminated PPeF, previously synthesized by a two-step melt polycondensation, another facile, solvent-free and industrially scalable process.

Experimental

Materials. Poly(L-lactic acid) in pellets (number average molecular weight determined by GPC: 55500 g/mol) (PLLA) (Corbion, Amsterdam, The Netherlands); 2,5-Furandicarboxylic acid 98% (2,5-FDCA) (Carbosynth Ltd., Compton, Berkshire, UK); 1,5-pentanediol 97% (1,5-PeD), hexamethylene diisocyanate ≥99% (HDI), titanium tetrabutoxide 97% (TBT), titanium isopropoxide 97% (TIP) (Sigma-Aldrich, Saint Louis, MO, USA).

Poly(L-Lactic Acid) Functionalization. OH-terminated poly(L-lactic acid) (PLLA-OH) was synthesized in a 250 mL stirred glass reactor put in a thermostated bath, starting from pellets of high-molecular-weight PLLA. 10 g (0.139 mol of repeating units) of PLLA were melted under nitrogen flow at 190 °C. Then, 6 g of PeD (0.058 mol) and TBT (200 ppm) were quickly added and mixed with PLLA for 2 minutes.

2,5-Furandicarboxylic Acid Esterification. The esterification of 2,5-FDCA was carried out into a round-bottom flask containing 25 g (0.160 mol) of the diacid and a large excess of methanol (390 mL, 9.64 mol, 1:30 molar ratio). As reported in the literature[30,35], the suspension became a solution after heating at 70 ° under magnetic stirring for 30 minutes. The flask was cooled down to room temperature, then 28 mL of thionyl chloride (1:1 molar ratio with respect to the -COOH groups) were added slowly because of the exothermic nature of the reaction. The suspension was heated again at 70 °C under stirring for three additional hours, and during this time, it turned into a pale yellow solution. The flask was finally cooled down in ice for 30 minutes, observing the crystallization of dimethyl furan-2,5-dicarboxylate (DMF). The product was vacuum filtered and washed multiple times using cold methanol. The final product, glossy white flakes of crystalline solid (22 g, 0.119 mol, corresponding to a yield of 74%), was dried overnight under a fume hood and stored under vacuum before use.

Poly(Pentamethylene 2,5-Furanoate) Synthesis. The synthesis of OH-terminated poly(pentamethylene 2,5-furanoate) (PPeF-OH) was carried out in a 250 mL stirred glass reactor put in a thermostated bath, following the usual polycondensation conditions for furan-based polyesters[30,34], starting from 5 g of DMF (0.027 mol), 11 g (0.106 mol) of 1,5-PeD (glycol excess of 400 mol%) and 200 ppm of both TBT and TIP, used as catalysts. The first step (transesterification

stage) was carried out at 190 °C under a flow of nitrogen for 3 hours, while methanol was distilled off. The second step (polycondensation stage) was carried out under vacuum in order to increase the molecular weight of the product. The temperature was raised from 190 up to 220 °C, while the pressure was lowered to 10 mbar, then slowly decreased to 0.05 mbar over the course of 2 hours, observing the gradual increase in the torque value. The synthesis was stopped once a constant value of the measured torque was recorded. Afterwards, in order to purify the as-synthesized pre-polymer, this last was dissolved in chloroform and precipitated in methanol. The material was stored under vacuum for 2 days before use.

Multiblock Copolymer and Chain-Extended PLLA Syntheses. The synthesis of the multiblock copolymer P(LLA50PeF50)-CE was carried out in a 250 mL stirred glass reactor put in a thermostated bath, according to the chain-extension conditions previously adopted for similar multiblock polyesters[26], starting from 1.5 g of PPeF-OH and 1.5 g of PLLA-OH. The reagents were melted under vacuum at 195 °C. At this point, the reactor was removed from the thermostated bath in order to decrease its temperature. 100 μL of hexamethylene diisocyanate (HDI) were added (30% molar excess with respect to the terminal -OH determined by ^{1}H-NMR analyses of the pre-polymers). The reaction was interrupted 3 minutes after the addition of HDI, as soon as torque value increased, to prevent side-reactions could take place[40]. Then, the product was purified by dissolution in chloroform and precipitation in methanol and stored under vacuum.

For the sake of comparison, chain-extended PLLA (PLLA-CE) was also prepared starting from PLLA-OH, following the same HDI chain-extension method.

Molecular Characterization. Proton- and carbon- nuclear magnetic resonance spectroscopy (^{1}H-NMR and ^{13}C-NMR) were performed using a Varian Inova 400-MHz (Agilent Technologies, Palo Alto, CA, USA) at room temperature. Samples were prepared by dissolving 10 mg of polymer for ^{1}H-NMR and 40 mg for ^{13}C-NMR in 0.7 mL of deuterated chloroform, containing 0.03 vol % of tetramethylsilane as an internal standard.

Gel-permeation chromatography (GPC) was used to determine the number average molecular weight (M_n) and the polydispersity index (D) of the polymers under study, using a 1525 binary HPLC pump (Waters, Milford, MA, USA) equipped with PLgel 5 mm MiniMIX-C column (Agilent Technologies), at 30 °C. Filtered HPLC-grade chloroform was used as eluent, and it was pumped into the system at a rate of 1 mL/min. Samples were prepared by dissolving the polymers in HPLC-grade chloroform (3 mg/mL). The calibration curve was obtained using polystyrene standards in the 800 – 100,000 g/mol range.

Film Preparation. P(LLA50PeF50)-CE, PLLA-CE and PPeF-OH were processed by compression molding using a C12 laboratory press (Carver, Wabash, IN, USA), obtaining 100 μm

thick free-standing films. About 2.5 g of purified polymer were placed between two Teflon sheets, which were positioned in the press and heated to a temperature 40 °C higher than their melting temperature for a minute, then the pressure was increased to 2 ton/m^2 for two minutes. The films were finally cooled to room temperature maintaining the same pressure. The as-obtained films were stored at room temperature, before performing characterization studies, to reach equilibrium crystallinity.

Thermal Characterization. Thermogravimetric analyses were performed on compression moulded films using a TGA4000 (PerkinElmer, Waltham, MA, USA). 5 mg of material were heated at a constant rate (10 °C/min), from 40 to 800 °C, under a pure nitrogen flow of 40 mL/min. $T_{5\%}$ was calculated as the temperature corresponding to a weight loss of 5%, T_{onset} was calculated as the temperature corresponding to the beginning of the weight loss, T_{max} was calculated as the minimum value of the derivative of the thermogram.

Calorimetric analyses were performed using a DSC6 (PerkinElmer, Waltham, MA, USA). 5 mg of polymeric films were placed in an aluminum pan and subjected to the following thermal program: 1. heating from -40 to 220 °C at 20 °C/min; 2. Isotherm for 3 minutes; 3. cooling from 220 to -40 °C at 100 °C/min; 4. isotherm for 12 minutes; 5. heating from -40 to 220 °C at 20 °C/min. The glass transition temperature (T_g) was calculated as the midpoint of the glass-to-rubber transition step; the specific heat increment (ΔC_p) was calculated as the height difference between the two baselines of the glass-transition step; the melting temperature (T_m) and the cold crystallization temperature (T_{cc}) were calculated as the peak maximum/minimum of the endothermic/exothermic phenomena in the DSC curve, respectively; the heat of fusion (ΔH_m) and heat of cold crystallization (ΔH_{cc}) were calculated from the total area of the endothermic and exothermic signals, respectively.

Structural Characterization. Wide-angle X-ray scattering (WAXS) measurements were performed using an X'PertPro diffractometer (PANalytical, Almelo, The Netherlands) equipped with a solid-state X'Celerator detector moving in 0.1° steps, at a rate of 100 s/step and with an X-ray source made of copper (wavelength = 0.15418 nm). The index of crystallinity (X_c) was calculated as the ratio between the crystalline diffraction area (A_c), obtained by subtracting the amorphous halo from the total area of the diffraction profile, and the total area (A_t) of the diffraction profile. Incoherent scattering was not taken into account in these calculations.

Mechanical Characterization. Tensile tests were performed using an Instron 5966 (Instron, Norwood, MA, USA) equipped with a transducer-coupled 1 kN load cell. Rectangular films (5 mm × 50 mm, gauge length of 20 mm) were stretched at a constant rate of 10 mm/min. The load-displacement curves were converted into stress-strain curves and the elastic modulus (E) was calculated as slope of the initial linear segment of the curve. At least five different tests were performed on each material under study, reporting the mean value ± standard deviation.

Permeability Tests. Permeability tests were performed using a permeance testing device, type GDP-C (Brugger Feinmechanik GmbH, Munchen, Germany) paired with an external thermostat HAAKE-Circulator DC10-K15 (ThermoFisher Scientific, Waltham, MA, USA). A manometric method was used in accordance with the Gas Permeability Testing Manual and to the standards ASTM D1434-82(2009) (*Standard test method for determining gas permeability properties of plastic film and coating*), DIN 53536 (*Determination of permeability of rubber to gases*) and ISO/DIS 15105-1:2007 (*Plastic film and sheeting determination of gas transport rate; part I: differential pressure method*). Each polymeric film (diameter of 10 cm, surface area of 78.5 cm^2) was placed between two chambers under the following conditions: pressure = 1 atm, temperature = 23 °C; gas flow = 100 cm^3/min, 0% relative humidity. The upper chamber was filled with the gas under investigation (pure O_2 or CO_2), while in lower chamber, a pressure transducer measured the increase in gas pressure as a function of time. Starting from the pressure-time plot, it was possible to calculate *gas transmission rate* (GTR) values, which represent the barrier properties of the film. Each measurement was performed in triplicate, reporting the mean value ± standard deviation.

Composting Tests. The compostability of P(LLA50PeF50)-CE, PLLA and PPeF was evaluated with a gravimetric method through a lab-scale experiment. Square samples (15 x 15 mm) were cut from a film of P(LLA50PeF50)-CE, weighed and placed in 100 mL jars, between two layers of hydrated mature compost (Nuova Geovis, Sant'Agata Bolognese, Italy) The composition of the used compost is indicated as follows: organic carbon 22.8% of the dry solid; humic and fulvic carbon: 13.44% of the dry solid; C/N rate: 12.97; pH: 8.15; salinity: 2.88 dS/m). The so-prepared samples were kept in a SW22 shaking water bath (Julabo GmbH, Seelbach, Germany) at 58 °C, with 90% relative humidity. At regular intervals, a pair of specimens was carefully withdrawn, washed with a 70% water/ethanol volumetric solution, dried in a fume hood for two days and weighed. The weight loss was calculated as:

$$((m_i - m_f) / m_i) \cdot 100$$

with m_i = initial weight, m_f = final weight. The results were collected as average value ± standard deviation, obtained from each pair of samples.

Partially degraded samples were also analyzed by means of ^{1}H-NMR, GPC, DSC and WAXS analyses, following the same procedures previously detailed. The samples were also subjected to a morphological investigation, using a S-2400 scanning electron microscope (Hitachi, Chiyoda, Tokyo, Japan), operating at 15 kV. The materials were sputter-coated with gold before examination.

Results and Discussion
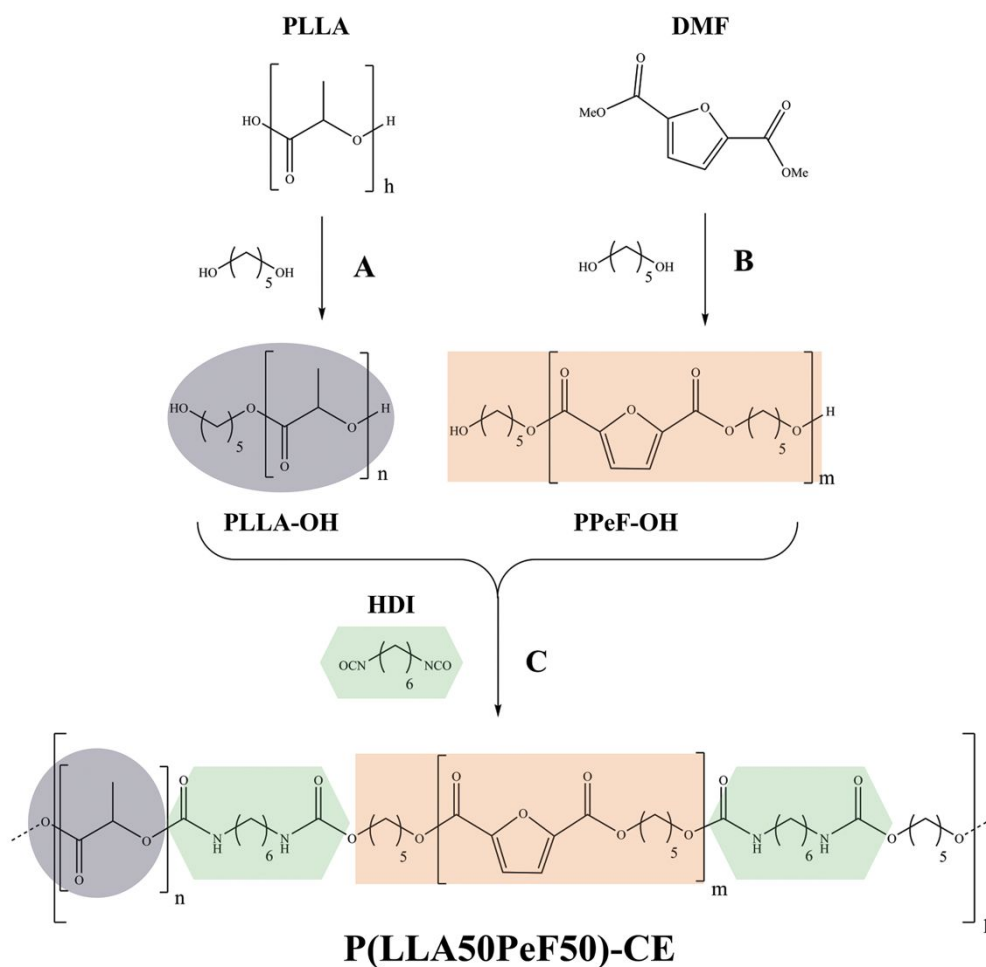
Scheme 1. Synthetic process followed to obtain the multiblock copolymer P(LLA50PeF50)-CE.

Molecular Characterization. The ^{1}H-NMR spectrum of PLLA-OH is represented in Figure 1, top panel. It is possible to observe the characteristic PLLA signals, such as the quadruplet at δ 5.19 ppm, corresponding to the internal -CH- proton (a) and the doublet at δ 1.59 ppm, associated to the internal methyl group (b). Four small additional peaks next to a and b signal, located at δ 1.41, δ 1.72, δ 4.98 and δ 5.35 ppm, respectively, can be also observed and ascribed to the the so-called carbon satellites, resulting from the coupling of ^{1}H atoms to an adjacent ^{13}C atom.

Furthermore, it is possible to note the presence of the triplet of the c protons at δ 4.15 ppm, and of the c' ones at δ 3.65 ppm, which correspond to the reacted pentanediol, while the signal of -CH$_2$O- from the unreacted diol PeD is superimposed to c' peak. The other two multiplets coming from the methylene groups of the reacted diol should be located at δ 1.85 and δ 1.55 ppm, but they appear to be covered by the b signal. It is also possible to note the presence of the a' quadruplet and of the b' doublet, respectively at δ 4.35 ppm and δ 1.50 ppm, associated to the OH-terminated LLA moieties. Lastly, the unreacted -COOH terminals can be derived from the intensity of the a'' quadruplet and

the b'' doublet, respectively located at δ 4.19 ppm and δ 1.50 ppm. From this spectrum, it was also possible to evaluate the average molecular weight of the polymeric chains (M_n), using the formula[41]:

$$M_n = DP \cdot W_{ur} \qquad (1)$$

where W_{ur} is the molecular weight of the repeating unit, and DP is the degree of polymerization corresponding to:

$$DP = [(I_{int} + I_{ext})/I_{ext}] \cdot 2 \qquad (2)$$

where I_{ext} is the normalized area of the proton signals from the three kinds of terminal units (a' + a'' + c), while I_{int} is the normalized area of the signal from the internal repeating units of PLLA (a). It was also possible to calculate the amount of -COOH terminals using the following equation:

$$COOH\% = I_{a''}/I_{ext} \cdot 100 \qquad (3)$$

where $I_{a''}$ is the normalized area of the signal from the -COOH terminals. The percentage of -COOH terminals in PLLA-OH was determined to be 35 mol%.

The ^{1}H-NMR spectrum of PPeF-OH is represented in Figure 1, central panel. The d singlet from the protons of the furanic ring is located at δ 7.20 ppm, while the signals from the methylenic protons of the glycolic subunit (e, f, g) are respectively registered at δ 4.35 ppm (triplet), δ 1.85 ppm (multiplet) and δ 1.55 ppm (multiplet). Apart from these signals ascribable to the internal repeating units, it is also possible to recognize the presence of a triplet at δ 3.65 ppm (e') originated from the methylene protons of the external glycolic subunits. From the ^{1}H-NMR spectrum, it was also possible to evaluate the average molecular weight for PPeF-OH using the above-mentioned equations (1) and (2). The result is in Table 1.

The ^{1}H-NMR spectrum of the chain-extended P(LLA50PeF50)-CE is represented in Figure 1, bottom panel. First of all, it is possible to observe the characteristic PLLA signals (a, b) and the peaks associated to the repeating units of PPeF (d, e, f, g), which confirm the presence of both homopolymers in the reaction product. New signals are also present (x, y, z, z') that can be associated to HDI: in particular, the z and z' protons are the ones belonging to the HDI which reacted with the OH groups of the PLLA and PPeF co-units, respectively. The composition of the copolymer was calculated from the integral ratio of the a and d signals originated from PLLA and PPeF protons, respectively. It was also possible to calculate the mass composition, multiplying the mole percentage of either co-unit by the molecular weight of the corresponding repeating unit. The result shows that lactic acid co-units amount is 54 wt% (75 mol%), thus the mass composition of the copolymer is very similar to the feed one (50 wt%).

In all spectra, the signal at 1.25 ppm can be attributed to the presence of silicone grease impurities. Table 1 also shows the molecular weights of P(LLA50PeF50)-CE and PLLA-CE, obtained from GPC analysis: the molecular weight of these samples is reasonably high and most importantly, higher than the molecular weight of the pre-polymers, confirming the successful control of the chain extension.
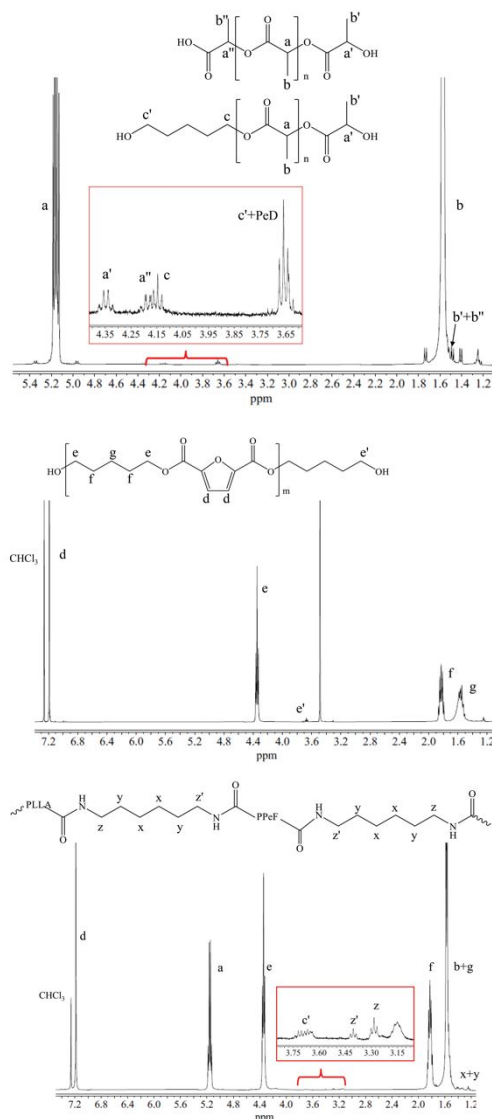

Figure 1. Top: ^{1}H-NMR spectrum of PLLA-OH with magnification of the region between 3.65 and 4.35 ppm; center: ^{1}H-NMR spectrum of PPeF-OH; bottom: ^{1}H-NMR spectrum of P(LLA50PeF50)-CE with magnification of the region between 3.15 and 3.75 ppm.

Table 1. Molecular (^{1}H-NMR and GPC), structural (WAXS) and thermal characterization (DSC and TGA) data of the polymers under study.

a: NMR b: GPC		WAXS	DSC						TGA		
M_n g/mol	Đ	X_c %	T_g °C	ΔC_p J/g°C	T_{cc} °C	ΔH_{cc} J/g	T_m °C	ΔH J/g	$T_{5\%}$ °C	T_{onset} °C	T_{max} °C

PLLA-OH	13500 [a]	-	20±1	58±1	0.035±0.005	81±1	5±1	173±1	39±2	269±2	318±2	344±1
II scan				58±1	0.338±0.005	-	-	-	-			
PPeF-OH	6900 [a]	-	7±1	13±1	0.179±0.003	-	-	66±1	16±1	358±2	368±2	390±1
II scan				13±1	0.338±0.004	-	-	-	-			
PPeF[30,35]	29600 [b]	2.4 [b]	-	13±1	0.394±0.004	-	-	-	-	-	392±2	414±2
II scan[30,35]				13±1	0.432±0.005	-	-	-	-			
P(LLA50PeF50)-CE	58700 [b]	3.6 [b]	-	21±1 59±1	0.155±0.003 0.205±0.003	101±1	14±1	169±1	15±1	282±1	286±2	308±1 391±1
II scan				22±1 59±1	0.159±0.003 0.157±0.003	104±1	14±1	169±1	15±1			
PLLA-CE	36700 [b]	2.4 [b]	-	58±1	0.279±0.004	100±1	30±2	168±1	36±2	270±1	306±2	345±2
II scan				58±1	0.301±0.004	97±1	28±2	166±1	36±2			

Thermal and Structural Characterization. The curves and the corresponding data from the TGA analysis are represented in Figure 2 and Table 1. The PPeF-OH sample is the most thermally stable among the ones under study, with a T_{max} of 390 °C, noticeably higher than the one of PLLA-OH (T_{max} = 351 °C). PLLA-OH shows an additional weight loss step of 5%, slightly above 100 °C, ascribed to the evaporation of absorbed humidity, which can be expected from a hygroscopic material such as low-molecular-weight PLLA. The same weight loss step due to water is not detected in the case of high molecular weight PLLA-CE, but apart from this difference, the thermal degradation profile and the T_{max} of PLLA-CE are very similar to the ones of PLLA-OH. The thermogravimetric curve of P(LLA50PeF50)-CE is intermediate between the ones of the two parent homopolymers: its thermal stability is improved with respects to PLLA because of the presence of PPeF blocks which degrade at higher temperature. While all the homopolymers under study degrade in a single step, the copolymer shows two distinct weight loss steps: the first one (T_{max} = 308 °C), could be attributed to PLLA blocks degradation, while the one at higher temperature (T_{max} = 391 °C) might be attributed to degradation of PPeF sequences. Observing the residual weight, it can be noted that PLLA-OH and PLLA-CE lose 100% of their initial weight, while in case of PPeF-OH a char residue of about 10% of the initial weight is measured. The chain extended polymer has an intermediate behavior, with a char residue that is about 8% of the initial weight of the sample. From the TGA results it can be inferred that the copolymerization of PLLA with PPeF caused an improvement in the underperforming thermal stability of PLLA.
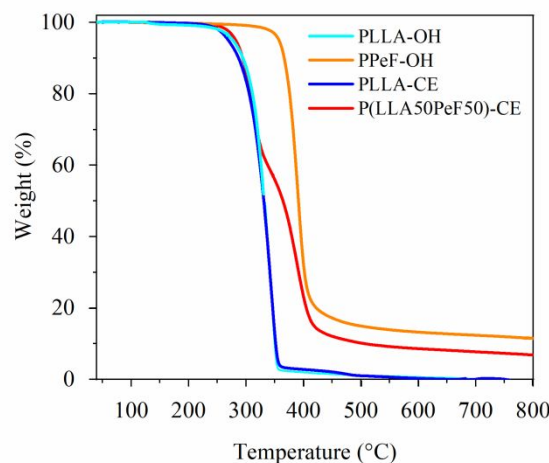
Figure 2. TGA curves of PLLA-OH, PPeF-OH, PLLA-CE and P(LLA50PeF50)-CE acquired by heating the polymers from 50 to 800 °C at 10 °C/min under nitrogen flow (40 mL/min).

The traces and data obtained from DSC analysis are presented in Figure 3 and Table 1. From the first scan (Figure 3, panel A), it can be noted that the OH-terminated, low molecular weight samples are semi-crystalline: their calorimetric curves show an endothermic variation of the baseline, associated to glass-to-rubber transition, followed by an endothermic melting peak. PPeF-OH presents a T_g value lower than room temperature, which indicates a high mobility of the amorphous phase, while PLLA-OH is characterized by a T_g equal to 58 °C, which implies the presence of a glassy amorphous phase at room temperature. The endothermic phenomena observed during the first DSC scan on PLLA-OH and PPeF-OH can be attributed to the melting of a crystalline phase whose formation might be favored by the purification process. In the case of PLLA-OH, a small exothermic crystallization phenomenon can be observed in the temperature range between T_g and T_m: apparently, above T_g, the macromolecules gather enough energy to organize and crystallize. In any case, being the exothermic cold-crystallization enthalpy (ΔH_{cc}) much lower than the endothermic melting enthalpy (ΔH_m), the material can be considered semi-crystalline, since only a negligible percentage of the crystalline phase formed over the course of the DSC analysis. During the second scan, (Figure 3, panel B), PPeF-OH appears to be completely amorphous, while PLLA-OH shows a behavior that is similar to the one previously observed in the first scan. In the case of PLLA-CE, the DSC analysis was carried out immediately after the compression molding of the material. PLLA-CE is characterized by a T_g well above room temperature, thus at this temperature its polymeric chains are frozen in their glassy state and they are not able to reorganize. On the other hand, P(LLA50PeF50)-CE has a T_g which is lower than room temperature and can undergo crystallization over time. For this reason, P(LLA50PeF50)-CE film was stored in a dryer for a month, in order to allow the possible development of a crystalline phase. From Figure 3, panel A, it can be noted that PLLA-CE shows a DSC profile which is similar

to the corresponding OH-terminated pre-polymer: an endothermic variation of the baseline corresponding to the T_g, associated with a clear physical aging phenomenon, is present, followed by an endothermic peak at higher temperature due to the melting of the crystalline phase. The presence of an exothermic peak between T_g and T_m indicates also a cold-crystallization process which occurs during heating. In this case, the exothermic crystallization enthalpy (ΔH_{cc}) is only slightly lower than the endothermic melting enthalpy (ΔH_m), confirming the almost-completely amorphous nature of the polymer, unlike the corresponding OH-terminated pre-polymer. Such a difference in the ability to crystallize can be attributed to the higher molecular weight of the chain-extended polymer. During the second scan (Figure 3, panel B), the behavior of the material does not manifest significant variations. As far as the multiblock copolymer is concerned, two distinct glass-transition temperatures were observed, indicating the presence of two amorphous phases with different chain mobility. The T_g which manifests at higher temperature (coupled with a physical aging phenomenon), coincides with the T_g of the PLLA-OH homopolymer and corresponds to the amorphous phase of PLLA. The T_g at lower temperature (also with physical aging), is observed at a higher temperature than the T_g of the PPeF-OH homopolymer: this might indicate that the amorphous phase of PPeF is partially miscible with PLLA, thus the small percentage of PLLA mixed with PPeF shifts the T_g to a temperature higher than the T_g of pure PPeF. During the second scan, after a rapid cooling from the melt (Figure 3, panel B), the two distinct glass-transition phenomena are still present, at temperatures similar to the ones of the first scan. The multiblock copolymer also shows an exothermic peak around 100 °C, (similar to the one of PLLA-CE) and an endothermic peak at 169 °C: these are related to the cold-crystallization and subsequent melting of the PLLA segments, and since the energy associated to both the events is about the same (14 vs 15 J/g, respectively), the material can be considered completely amorphous. It is interesting to note that the value of ΔH_m of the copolymer is about half the ΔH_m of PLLA-CE, coherently with the mass composition deduced from both the ^{1}H-NMR spectra (Figure 1, bottom panel) and the TGA thermogram (Figure 2). During the second scan (Figure 3, panel B), P(LLA50PeF50)-CE shows a behavior similar to the one observed during the first scan.

Wide-angle X-ray analysis (WAXS) was carried out in order to ascertain the nature and the percentage of the crystalline phase present in the polymers under study. The resulting diffraction diagrams are shown in Figure 3, panel C, while the degree of crystallinity X_c is listed in Table 1. The patterns of the two OH-terminated samples are typical of semi-crystalline materials, in agreement with DSC measurements: they show some reflections originated from the crystalline phase of the material, superimposed to a bell-shaped baseline associated to the amorphous phase. In the case of PLLA-OH, such reflections appear sharper (the main ones are located at $2\theta = 17$ and 19 °), while in the case of PPeF-OH, the reflections emerge only partially from the amorphous bell, further proving

that, in this case, the degree of crystallinity is lower. Only a bell-shaped baseline can be noted in the diffractograms of both the chain-extended polymers, indicating a fully amorphous nature. This is in accordance with the results of DSC analysis, albeit the position and the profile of the bell-shaped segments are different in the two cases: the bell-shaped curve of PLLA-CE is centered at lower angles (thus meaning higher mean spacing) than the one of the multiblock copolymer.
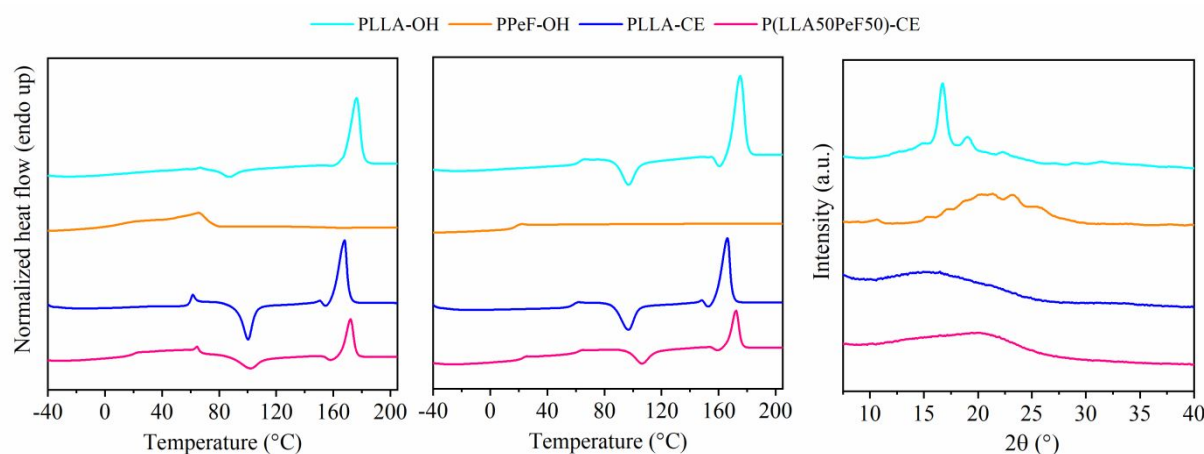

Figure 3. I DSC scan (left panel), II DSC scan (center panel) and WAXS patterns (right panel) of PLLA-OH (light blue), PPeF-OH (orange), PLLA-CE (blue) and P(LLA50PeF50)-CE (pink) films. The heat flow measured by the instrument was normalized by dividing for the weight of the sample.

Mechanical Characterization. Tensile tests were performed only on the chain-extended materials, being the only with a value of molecular weight high enough for this kind of measurements. Their stress-strain curves are represented in Figure 4, together with the curve of high-molecular-weight PPeF[30,35]. The experimental values of elastic modulus (E), stress at break (σ_b) and elongation at break (ε_b) are shown in Table 2, together with the ones of high-molecular-weight PPeF[30,35]. It can be noted that PLLA-CE is characterized by high elastic modulus and stress at break, paired with almost no elongation at break, confirming its remarkable rigidity. The fact these parameters are significantly different in the multiblock copolymer can be attributed to the introduction of PPeF in the polymeric structure. In fact, PPeF is an elastomeric material in a rubbery amorphous state at room temperature, characterized by an outstanding elongation at break, by an instant shape recovery and by a low elastic modulus. All these properties were attributed to the presence of a 2D-ordered phase originated from inter-chain hydrogen bonds as well as π-π interactions[35]. As a matter of fact, the presence of PPeF sequences in the block copolymer leads to a decrease of about 75% of the elastic modulus, compared to the one of PLLA-CE, and to a halved stress at break. At the same time, the elongation at break of PLLA-CE is significantly improved in the multiblock copolymer, increased from 1% to more than 150%. The properties of the copolymer are intermediate between the ones of

the reference homopolymers, and this cannot be explained on the basis of a different type and degree of crystallinity, since all the polymers are amorphous. The physical mixing of the two homopolymers of reference, physical blend of PLLA and PPeF (with comparable composition, and degree of crystallinity compared to P(LLA50PeF50)-CE) have already been studied[22] and resulted in significantly inferior mechanical properties compared to P(LLA50PeF50)-CE, demonstrating the successful of the chain extension reaction performed to obtain P(LLA50PeF50)-CE was. The higher rigidity of PLLA-CE can be attributed to its glassy state, while in the multiblock copolymer, the presence of flexible segments in a rubbery state at room temperature contributes to significantly reduce the rigidity imparted by PLLA. Contrary to PPeF, P(LLA50PeF50)-CE shows no shape recovery after the yield point (measured at a deformation of about 7%). Overall, the copolymerization of PLLA with PPeF determined a significant decrease in the rigidity and fragility of PLLA together with an important improvement of the elongation.
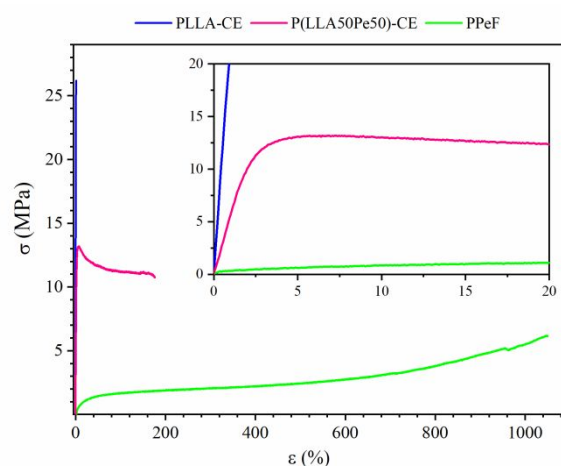

Figure 4. Stress-strain curves of PPeF[30,35], PLLA-CE and P(LLA50PeF50)-CE. In the inset: magnification of the curves at low strain values.

Table 2. Mechanical characterization data.

Polymer	E (MPa)	σ_b (MPa)	ε_b (%)
PLLA-CE	2052 ± 93	23.4 ± 2.5	1.2 ± 0.1
P(LLA50PeF50)-CE	535 ± 58	10 ± 1	162 ± 22
PPeF[30,35]	9 ± 1	6.1 ± 0.5	1050 ± 200

Gas-Barrier Properties Evaluation. The results of the permeability tests for P(LLA50PeF50)-CE and PLLA-CE are expressed as Gas Transmission Rates (GTR) and compared in Figure 5 with the GTR values of some polyolefin commodities, widely used in the food packaging industry: poly(propylene) (PP), high-density poly(ethylene) (HDPE) and low-density poly(ethylene) (LDPE)[42].

P(LLA50PeF50)-CE shows O_2- and CO_2-transmission rates of 2.04 ± 0.01 and 6.89 ± 0.01 cm^3 cm / m^2 d atm, respectively, about 35-40% lower than the ones of PLLA-CE, which are 3.51 ± 0.01 and 10.50 ± 0.01 cm^3 cm / m^2 d atm, respectively. The improvement cannot be explained on the basis of a difference in free volume of the amorphous phase: in fact, PLLA-CE is characterized by an amorphous phase with lower free volume, since its T_g is higher than the one of P(LLA50PeF50)-CE at room temperature. On the other hand, the multiblock copolymer has two distinct T_g temperatures, one of which is below room temperature (the one of the phase rich in PPeF). The presence of PPeF, analogously to the mechanical response enhancement, provides an improvement of the gas barrier capability, too. The outstanding gas-barrier properties of PPeF have been attributed to the formation of a 2D-ordered mesomorph phase, whose formation could be promoted by the formation of hydrogen bonds and π-π interactions between adjacent polymer chains[35]. The presence of such a phase in P(LLA50PeF50)-CE would explain the improvement in gas-barrier properties when compared to PLLA-CE. As shown in Figure 5, it can be observed that the gas barrier of the multiblock copolymer is clearly superior to the ones of commercial polyolefins. These results highlight P(LLA50PeF50)-CE as a promising candidate for the production of flexible, monolayer, ecologically-sustainable films for food packaging.
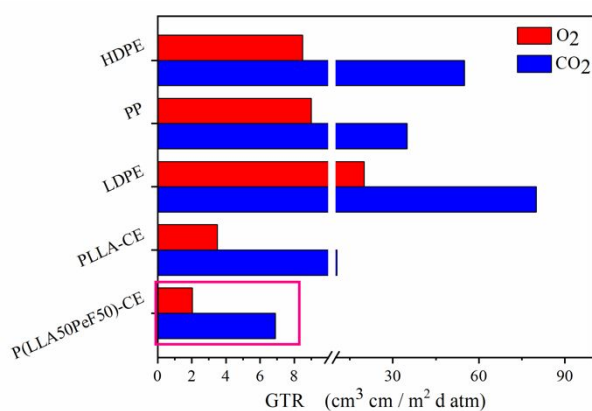

Figure 5. O_2 and CO_2 transmission rates at 23 °C in dry (0% RH) atmosphere for P(LLA50PeF50)-CE and PLLA-CE, compared with HDPE, LDPE and PP[42].

Composting Tests. PLLA-CE, P(LLA50PeF50)-CE and PPeF[30,35] were subjected to composting tests. With the aim of achieving a greater understanding of the degradation process, for all the three polymers, the specimens withdrawn at different times have been subjected to gravimetric weight loss determination and molecular (^{1}H-NMR and GPC), structural (WAXS) and thermal (DSC) characterization. Moreover, SEM microscopy has been employed to follow the surface evolution in composted films. Finally, in addition to the incubated samples (subject to temperature annealing,

humidity and attack from microorganisms), specimens exclusively subjected to thermal treatment and moisture (blanks, maintained at 58 °C) were studied.

As concerns weight loss, a general increasing trend was evidenced, although the samples incorporated compost, especially for long incubation times, compromising the accuracy of the gravimetric weight measurements. Nevertheless, a 100% weight loss was registered at 41 days for PLLA-CE and 56 days for PPeF and P(LLA50PeF50)-CE. As it can be noted from the macroscopic and the microscopic pictures in Figure 6, the surface of the compression-molded film samples was initially smooth and homogeneous, while partially-degraded samples showed a progressive fragmentation which increased with incubation time. In all cases, the materials became progressively more opaque and more fragile (Figure 6).

As for the SEM microscopies (Figure 6, right side), two different behaviors can be noticed for the two homopolymers at 21 days of composting time: PLLA-CE shows large and deep cracks throughout its surface, while PPeF shows shallow scratches and small dimples. The multi-block copolymer seems to have intermediate behavior, showcasing deep dimples and cracks.
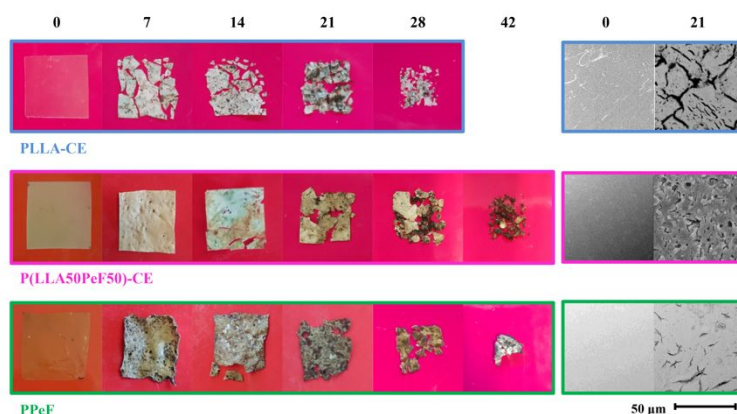

Figure 6. Macroscopic (left) and SEM (right) pictures of PLLA-CE, P(LLA50PeF50)-CE and PPeF samples after a composting treatment of different duration, expressed in days.

Further proof of the degradation of P(LLA50PeF50)-CE and of its parent homopolymers came from GPC analysis: Table 3 shows a progressive decrease of the molecular weight of the incubated samples compared to the original molecular weight (M_n/M_{n0}), paired with a gradual increase in polydispersity (Đ). It is interesting to note that the decrease in molecular weight (Figure 7, left panel) and the increase in polydispersity (Figure 7, center panel) takes place at different rates for the three materials: slowest for PPeF, fastest for PLLA-CE and intermediate for P(LLA50PeF50)-CE. This result is clear also from Figure 8, where the chromatograms of the three polymers, at different incubation times, are reported as a function of retention time. In the case of PLLA-CE (left panel of Figure 8), the signal

moves towards higher retention times (i.e. lower molecular weight) with incubation time and a shoulder develops at higher retention time, being the side peak even more intense than the main one after 28 days of composting. A similar evolution can be highlighted for P(LLA50PeF50)-CE, while it is absent in the case of PPeF.

Table 3. GPC, ^{1}H-NMR, DSC and WAXS data on partially degraded samples subjected to composting treatment, and on blank samples which were not in contact with compost.

| Composting time Days	GPC		^{1}H-NMR	DSC		WAXS
	M_n/M_{n0} %	Đ	PPeF wt%	T_m °C	ΔH_m J/g	X_c %
PLLA-CE						
14 (blank)	-	-	-	164	49	-
7	86	2.1	0	164	40	30±2
14	50	2.4	0	165	40	30±1
21	42	3.5	0	162	48	34±4
28	37	4.2	0	162	49	35±3
PPeF[30,35]						
14 (blank)	-	-	-	54 84	2 27	-
4	96	2.0	100	55 85	4 17	14±1
7	78	2.1	100	55 85	4 18	14±1
14	84	2.2	100	55 85	4 20	16±1
21	72	2.2	100	55 85	4 22	16±1
35	68	2.5	100	56 85	4 24	17±1
P(LLA50PeF50)-CE						
21 (blank)	-	-	46	84 168	13 21	19±2
2	98	2.1	39	168	17	18±3
4	91	2.2	34	167	18	18±3
7	90	2.3	35	85 167	1 20	18±3
14	74	2.6	37	84 166	4 22	20±2
21	58	2.8	41	86 163	9 24	23±5
23	50	3.5	46	86 156	10 22	22±3
28	47	3.9	52	86 153	10 20	20±3
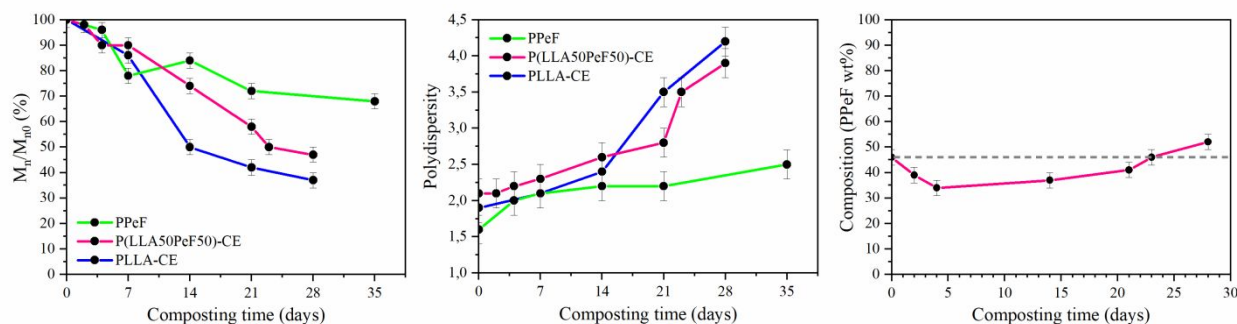
Figure 7. Variation of molecular weight (left panel), polydispersity (center panel) and composition of P(LLA50PeF50)-CE (right panel) after composting treatment with a duration expressed in days.
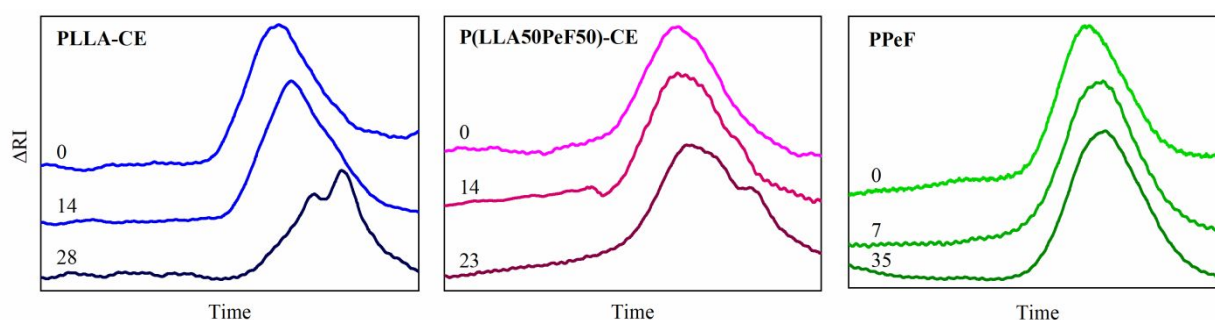

Figure 8. GPC elugrams on samples of PLLA-CE (left panel), P(LLA50PeF50)-CE (center panel) and PPeF (right panel), after composting treatment with a duration expressed in days. ΔRI is the measured difference in refractive index.

^{1}H-NMR analysis was also carried out on partially degraded samples of P(LLA50PeF50)-CE: Table 3 and Figure 7 (right panel) show the weight percentage composition of the copolymer, obtained from the integral ratio of the a and d signals, respectively, originated from PLLA and PPeF protons (Figure 1, bottom panel). The results show a reduction of PPeF blocks, reaching a minimum of 34 wt% after 4 days of composting. Table 3 and Figure 7 also show that, for longer composting times (23 days), composition returns to its initial value (46 wt%).

As previously mentioned, the partially degraded samples of P(LLA50PeF50)-CE, PLLA-CE and PPeF were subjected to DSC analyses (Figure 9). All the samples, initially amorphous, crystallized during incubation, as it is possible to observe by comparing the melting peak intensities (Figure 9) and enthalpies of the neat polymers (Table 1), the incubated materials and the blanks (Table 3). All the endothermic peaks were confirmed to be originated by the thermal/composting treatment, except for the small PPeF peak located at 55 °C, which was found to be a room-temperature-annealed phase, evolving after the withdrawal of PPeF samples from compost. The comparison between blanks and the samples at equal time of treatment (Figure 9 and Table 3) shows that the melting enthalpy is similar, even though the melting peaks of the samples subjected to composting treatment showcase

an evolving shape, while the DSC curves of the blanks remain similar throughout the experiment. More in detail, the shape and position of the endothermic peak at 85 °C, detected in PPeF homopolymer trace, did not change over time (Figure 9 and Table 3). Conversely, the endotherm due to the crystalline phase present in PLLA-CE, originally at 168 °C (Figure 9 and Table 1), shifted towards lower melting temperatures (Figure 9 and Table 3) and a side peak developed with the increasing composting times. As expected, all of the above mentioned thermal phenomena of PPeF and PLLA-CE and their evolution (or lack thereof) over time are found in the thermograms of P(LLA50PeF50)-CE (Figure 9, central panel).
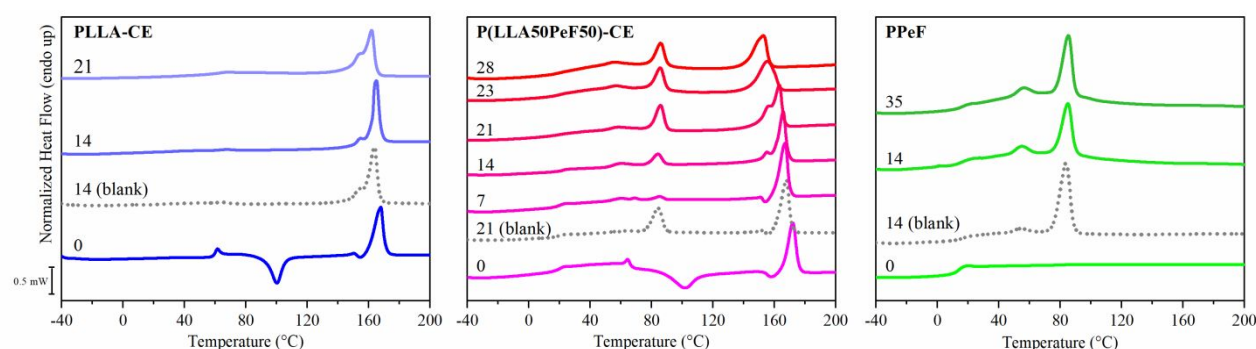

Figure 9. I DSC scans of PLLA-CE (left panel), P(LLA50PeF50)-CE (center panel) and PPeF (right panel) after composting treatment with a duration expressed in days. The heat flow measured by the instrument was normalized by dividing for the weight of the sample.

Partially degraded samples were also analyzed by WAXS. Figure 10 compares P(LLA50PeF50)-CE composted for 2 and 21 days with PLLA-CE and PPeF composted for 14 days. After 2 days of treatment, P(LLA50PeF50)-CE only shared diffractometric reflections with crystalline PLLA-CE (main peaks at $2\theta = 16.5$ °, 18.9 °, 24.5 °, 28.8 °), while at 21 days of treatment, the diffractometric reflections of PPeF in P(LLA50PeF50)-CE became more evident ($2\theta = 10.8$ °; 18.2 °; 23.6 °). WAXS analyses showed an increase in the degree of crystallinity. This is clearly visible in Figure 10, which shows the sharper crystalline reflections over the amorphous halo of P(LLA50PeF50)-CE incubated for 21 days, compared to P(LLA50PeF50)-CE incubated for 2 days.
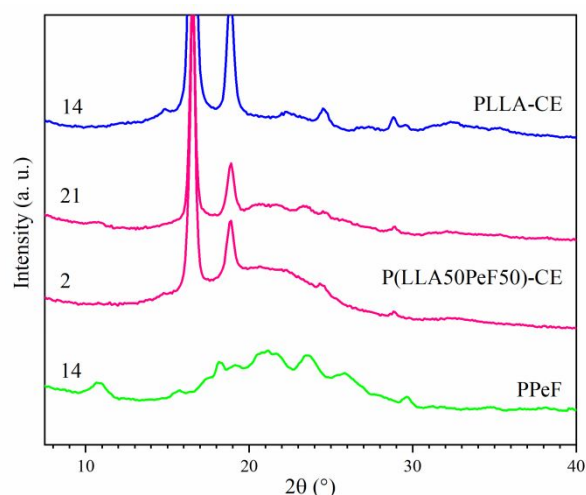
Figure 10. WAXS diffractograms of composted PPeF (green), PLLA-CE (blue) and P(LLA50PeF50)-CE (pink), after composting treatment with a duration expressed in days.

Overall, the results which were gathered on samples subjected to composting treatment allowed the achievement of interesting conclusions on the degradation kinetics and mechanism of the polymers under study, which are represented in Scheme 2.

In terms of kinetics, a first information is provided by the fragmentation rate observed for the three polymers (Figure 6, left) and by the SEM surface images (Figure 6, right), both suggesting a slower degradation for PPeF, in line with previous works highlighting the higher stability of aromatic polymers under composting conditions, compared with aliphatic ones[43].

Additionally, the results obtained seem to suggest that the amorphous phase degraded more rapidly, when compared to the crystalline phase, this last being attacked once the process is well underway. A significant contribution of thermal annealing at 58 °C could be responsible for the evolution of a higher crystalline / amorphous ratio, but it is reasonable to believe that the amorphous phase of polyesters should also be subjected to a greater rate of degradation, because it is more readily permeated by water molecules and enzymes, as reported in the literature[43]. In any case, the enhancement of the crystalline phase, more pronounced for PLLA, followed by the block copolymer and then by PPeF, was confirmed by several findings:

- Visually (Figure 6), the samples subjected to composting treatment were found to become more opaque;
- In DSC analyses, the samples subjected to composting treatment were found to be strongly crystalline (Table 3 and Figure 9), while the original samples were not (Table 1 and Figure 3); the lowering of melting temperature as well as the appearance of a shoulder on the endotherm, testify the attack, at longer incubation times, of the crystalline fraction as well.

- ▪ In WAXS analyses (Figure 10), the amorphous halo became less pronounced when compared to the crystalline peaks, for higher composting times.

Although, as already mentioned, PLLA is the most crystalline sample and the only one with a glassy amorphous phase among the family, it is the fastest degrading material. Therefore, it seems that crystallinity is not the main parameter affecting the degradation rate, but rather the density of ester groups, which is higher in PLLA chains than in PPeF and P(LLA50PeF50)-CE ones.

In terms of mechanism, overwhelming evidence was gathered to support the claim of a superficial erosion mechanism for PPeF and a bulk hydrolysis mechanism for PLLA. Specifically:

- ▪ In SEM analyses (Figure 6, right side), the cracks shown for PLLA-CE samples subjected to composting treatment are typical of polyesters partially degraded through a bulk hydrolysis mechanism, in which the degradation of the sample takes place at the same time from inside and on the surface of the sample[43]. On the other hand, the shallow dimples and scratches shown for PPeF are typical of a polyester partially degraded in a surface erosion mechanism, in which only the surface of the sample is accessible to enzymes[43,44]. Finally, in the case of the copolymer, an intermediate behavior is shown, as expected.

- ▪ In GPC analyses (Figure 8 and Figure 7), the side peak developed after composting treatment and the progressive shift of the peaks, as seen in PLLA-CE and P(LLA50PeF50)-CE is likely due to the accumulation of lower molecular weight fractions produced by hydrolysis of the lactic -COOR groups, in line with a bulk degradation process typical of PLLA. In this case, the fractions with lower molecular weight remain trapped inside the sample being in fact detected by GPC analyses[43]. The absence of such phenomena in PPeF can be explained considering a degradation mechanism that takes place by surface erosion: in this case, the polymeric fractions with lower molecular weight were dispersed in the compost as the degradation process progresses, and as such, they likely remained inside the compost matrix upon extraction of the sample and were not detected by means of GPC. As a factual consequence, during GPC analyses PPeF samples show a lower decrease in molecular weight, a lower increase in polydispersity and no side peak development.

- ▪ In NMR analyses (Figure 7, right panel), the composition of P(LLA50PeF50)-CE was shown to change over time, after composting treatment. However, aromatic polyesters are known to be less readily compostable than aliphatic ones by means of enzymatic hydrolysis[43], so the decrease in percentage of PPeF should not be explained as a difference in degradation rate, but rather as a consequence of the different degradation mechanism: since PPeF degrades following a surface erosion mechanism, the PPeF fractions are the first to leave the sample and are lost in the compost matrix. When, at higher composting times, the composition returns

to its original value, the phenomenon is likely caused by a faster rate of degradation of PLLA. This observation is supported by the literature[12]: the biodegradation mechanism of PLLA is initially driven by the hydrolytic cleavage of ester bonds in the amorphous regions of the material and the kinetics of this first step is not linear, since the increasing concentration of carboxylic acid terminals self-catalyzes the reaction and progressively increases the rate of degradation. When the molecular weight becomes lower than 20,000 g/mol, PLA becomes hydrophilic and the second stage of the process begins, with the contribution of microorganisms, which metabolize low-molecular-weight PLA into carbon dioxide, water and biomass. Overall, the degradation of P(LLA50PeF50)-CE is led by the bulk hydrolysis of PLLA segments and by the surface erosion of PPeF ones, causing the composition of the copolymer to change accordingly.
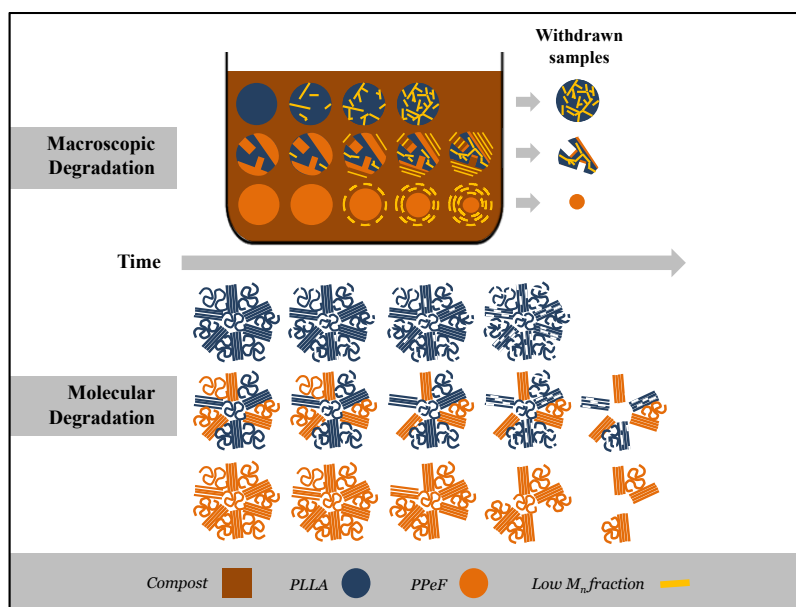
Scheme 2. Schematization of the degradation mechanism and kinetics of PLLA, P(LLA50PeF50)-CE and PPeF.

Conclusions

The eco-design of an aromatic-aliphatic multiblock copolyester, P(LLA50PeF50)-CE, based on poly(lactic acid) and containing furan moieties, was carried out with the aim of improving the properties of poly(L-lactic acid) for sustainable food packaging applications. The innovative synthetic method used is in line with the principles of Green Chemistry, being solvent-free and starting from biobased reagents. With it, it was possible to overcome key limitations of PLLA, using 2,5-furandicarboxylic acid as comonomer. Specifically:

- The thermal stability of PLLA was improved;
- The stiffness and brittleness of PLLA were drastically reduced, allowing the copolymer to be processed into films for flexible packaging applications;
- The oxygen permeability of PLLA was decreased of about 40% and a similar improvement was also achieved towards carbon dioxide;
- The biodegradation of PLLA was not compromised, since film samples of both the multiblock copolymer and of its parent homopolymers were fully degraded within 60 days of composting treatment.

The in-depth study of the composting process has led to the conclusion that the PLLA and PPeF degraded through a bulk hydrolysis and a superficial erosion mechanism, respectively, being PLLA the faster degrading component. The results stress the great potential of P(LLA50PeF50)-CE as biobased and biodegradable bioplastic with outstanding properties for flexible, monolayer and sustainable food packaging applications.

Author contributions

E.B. polymer synthesis; characterization; data curation; visualization; writing of original draft. G.G. polymer synthesis; characterization; data curation; visualization; correction and revision of the manuscript. M.S. conceptualization, supervision of experimental activity; analysis of the overall experimental data; writing of original draft, correction and revision of the manuscript. V.S. gas barrier measurements and data analysis; correction and revision of the manuscript. M.G. X-ray diffraction measurements and data analysis; correction and revision of the manuscript. E. S. data analysis; correction and revision of the manuscript. N.L. supervision of experimental activity; analysis of the overall experimental data; correction and revision of the manuscript; conceptualization and supervision of the work and research funding.

Conflicts of Interest

There are no conflicts to declare.

Acknowledgments

References

(1)   PlasticsEurope. *Plastics – the Facts 2022*. https://plasticseurope.org/knowledge-hub/plastics-the-facts-2022/ (accessed Feb 2, 2023).

(2)   European Bioplastics. Bioplastics market data. https://www.european-bioplastics.org/market/ (accessed Feb 2, 2023).

(3)   Genovesi, A.; Aversa, C.; Barletta, M.; Cappiello, G.; Gisario, A. Comparative Life Cycle Analysis of Disposable and Reusable Tableware: The Role of Bioplastics. *Clean. Eng. Technol.* **2022**, *6*, 100419. https://doi.org/10.1016/j.clet.2022.100419.

(4)   Siracusa, V.; Blanco, I.; Romani, S.; Tylewicz, U.; Rocculi, P.; Rosa, M. D. Poly(Lactic Acid)-Modified Films for Food Packaging Application: Physical, Mechanical, and Barrier Behavior. *J. Appl. Polym. Sci.* **2012**, *125* (S2), E390–E401. https://doi.org/10.1002/app.36829.

(5)   Ingrao, C.; Tricase, C.; Cholewa-Wójcik, A.; Kawecka, A.; Rana, R.; Siracusa, V. Polylactic Acid Trays for Fresh-Food Packaging: A Carbon Footprint Assessment. *Sci. Total Environ.* **2015**, *537*, 385–398. https://doi.org/10.1016/j.scitotenv.2015.08.023.

(6)   Ingrao, C.; Gigli, M.; Siracusa, V. An Attributional Life Cycle Assessment Application Experience to Highlight Environmental Hotspots in the Production of Foamy Polylactic Acid Trays for Fresh-Food Packaging Usage. *J. Clean. Prod.* **2017**, *150*, 93–103. https://doi.org/10.1016/j.jclepro.2017.03.007.

(7)   Rudnik, E.; Briassoulis, D. Comparative Biodegradation in Soil Behaviour of Two Biodegradable Polymers Based on Renewable Resources. *J. Polym. Environ.* **2011**, *19* (1), 18–39. https://doi.org/10.1007/s10924-010-0243-7.

(8)   Lasprilla, A. J. R.; Martinez, G. A. R.; Lunelli, B. H.; Jardini, A. L.; Filho, R. M. Poly-Lactic Acid Synthesis for Application in Biomedical Devices — A Review. *Biotechnol. Adv.* **2012**, *30* (1), 321–328. https://doi.org/10.1016/j.biotechadv.2011.06.019.

(9)   Tyler, B.; Gullotti, D.; Mangraviti, A.; Utsuki, T.; Brem, H. Polylactic Acid (PLA) Controlled Delivery Carriers for Biomedical Applications. *Adv. Drug Deliv. Rev.* **2016**, *107*, 163–175. https://doi.org/10.1016/j.addr.2016.06.018.

(10)   Pellis, A.; Malinconico, M.; Guarneri, A.; Gardossi, L. Renewable Polymers and Plastics: Performance beyond the Green. *N. Biotechnol.* **2021**, *60*, 146–158. https://doi.org/10.1016/j.nbt.2020.10.003.

(11)   Castro-Aguirre, E.; Iñiguez-Franco, F.; Samsudin, H.; Fang, X.; Auras, R. Poly(Lactic Acid)—Mass Production, Processing, Industrial Applications, and End of Life. *Adv. Drug*

Deliv. Rev. **2016**, *107* (April), 333–366. https://doi.org/10.1016/j.addr.2016.03.010.

(12)   Reichert, C. L.; Bugnicourt, E.; Coltelli, M.-B.; Cinelli, P.; Lazzeri, A.; Canesi, I.; Braca, F.;

Martínez, B. M.; Alonso, R.; Agostinis, L.; Verstichel, S.; Six, L.; Mets, S. D.; Gómez, E. C.;

Ißbrücker, C.; Geerinck, R.; Nettleton, D. F.; Campos, I.; Sauter, E.; Pieczyk, P.; Schmid, M.

Bio-Based Packaging: Materials, Modifications, Industrial Applications and Sustainability.

Polymers **2020**, *12* (7), 1558. https://doi.org/10.3390/polym12071558.

(13)   Vilela, C.; Sousa, A. F.; Fonseca, A. C.; Serra, A. C.; Coelho, J. F. J.; Freire, C. S. R.;

Silvestre, A. J. D. The Quest for Sustainable Polyesters-Insights into the Future. *Polym.*

Chem. **2014**, *5* (9), 3119–3141. https://doi.org/10.1039/c3py01213a.

(14)   Flexible Packaging Association. Resources on Sustainable Packaging

https://www.flexpack.org/resources/sustainability-resources#lca-case-studies (accessed Feb

2, 2023).

(15)   Wagner, J. R.; Marks, S. B. 1 - Introduction. In *Plastics Design Library*; Wagner, J. R. B. T.-

M. F. P. (Second E., Ed.; William Andrew Publishing, 2016; pp 3–13.

https://doi.org/10.1016/B978-0-323-37100-1.00001-6.

(16)   Werpy, T.; Petersen, G.; Aden, A.; Bozell, J.; Holladay, J.; White, J.; Manheim, A.; D., E.;

Lasure, L.; Jones, S.; Gerber, M.; Ibsen, K.; Lumberg, L.; Kelley, S. *Volume I: Results of*

Screening for Potential Candidates from Sugars and Synthesis Gas; Werpy, T., Petersen, G.,

Eds.; U.S. Department of Energy, 2004.

(17)   Sousa, A. F.; Vilela, C.; Fonseca, A. C.; Matos, M.; Freire, C. S. R.; Gruter, G. J. M.;

Coelho, J. F. J.; Silvestre, A. J. D. Biobased Polyesters and Other Polymers from 2,5-

Furandicarboxylic Acid: A Tribute to Furan Excellency. *Polym. Chem.* **2015**, *6* (33), 5961–

5983. https://doi.org/10.1039/c5py00686d.

(18)   Bianchi, E.; Soccio, M.; Siracusa, V.; Gazzano, M.; Thiyagarajan, S.; Lotti, N.

Poly(Butylene 2,4-Furanoate), an Added Member to the Class of Smart Furan-Based

Polyesters for Sustainable Packaging: Structural Isomerism as a Key to Tune the Final

Properties. *ACS Sustain. Chem. Eng.* **2021**, *9* (35), 11937–11949.

https://doi.org/10.1021/acssuschemeng.1c04104.

(19)   Quattrosoldi, S.; Guidotti, G.; Soccio, M.; Siracusa, V.; Lotti, N. Bio-Based and One-Day

Compostable Poly(Diethylene 2,5-Furanoate) for Sustainable Flexible Food Packaging:

Effect of Ether-Oxygen Atom Insertion on the Final Properties. *Chemosphere* **2022**, *291*,

132996. https://doi.org/10.1016/j.chemosphere.2021.132996.

(20)   Fredi, G.; Rigotti, D.; Bikiaris, D. N.; Dorigato, A. Tuning Thermo-Mechanical Properties of

Poly(Lactic Acid) Films through Blending with Bioderived Poly(Alkylene Furanoate)s with

Different Alkyl Chain Length for Sustainable Packaging. *Polymer (Guildf)*. **2021**, *218*, 123527. https://doi.org/10.1016/j.polymer.2021.123527.

(21)   Perin, D.; Fredi, G.; Rigotti, D.; Soccio, M.; Lotti, N.; Dorigato, A. Sustainable Textile Fibers of Bioderived Polylactide/Poly(Pentamethylene 2,5-Furanoate) Blends. *J. Appl. Polym. Sci.* **2021**, *139* (10), 51740. https://doi.org/10.1002/app.51740.

(22)   Rigotti, D.; Soccio, M.; Dorigato, A.; Gazzano, M.; Siracusa, V.; Fredi, G.; Lotti, N. Novel Biobased Polylactic Acid/Poly(Pentamethylene 2,5-Furanoate) Blends for Sustainable Food Packaging. *ACS Sustain. Chem. Eng.* **2021**, *9* (41), 13742–13750. https://doi.org/10.1021/acssuschemeng.1c04092.

(23)   Terzopoulou, Z.; Papadopoulos, L.; Zamboulis, A.; Papageorgiou, D. G.; Papageorgiou, G. Z.; Bikiaris, D. N. Tuning the Properties of Furandicarboxylic Acid-Based Polyesters with Copolymerization: A Review. *Polymers (Basel)*. **2020**, *12* (6), 1209. https://doi.org/10.3390/polym12061209.

(24)   Matos, M.; Sousa, A. F.; Fonseca, A. C.; Freire, C. S. R.; Coelho, J. F. J.; Silvestre, A. J. D. A New Generation of Furanic Copolyesters with Enhanced Degradability: Poly(Ethylene 2,5-Furandicarboxylate)-Co-Poly(Lactic Acid) Copolyesters. *Macromol. Chem. Phys.* **2014**, *215* (22), 2175–2184. https://doi.org/10.1002/macp.201400175.

(25)   Sousa, A. F.; Patrício, R.; Terzopoulou, Z.; Bikiaris, D. N.; Stern, T.; Wenger, J.; Loos, K.; Lotti, N.; Siracusa, V.; Szymczyk, A.; Paszkiewicz, S.; Triantafyllidis, K. S.; Zamboulis, A.; Nikolic, M. S.; Spasojevic, P.; Thiyagarajan, S.; van Es, D. S.; Guigo, N. Recommendations for Replacing PET on Packaging, Fiber, and Film Materials with Biobased Counterparts. *Green Chem.* **2021**, *23* (22), 8795–8820. https://doi.org/10.1039/D1GC02082J.

(26)   Guidotti, G.; Soccio, M.; Lotti, N.; Siracusa, V.; Gazzano, M.; Munari, A. New Multi-Block Copolyester of 2,5-Furandicarboxylic Acid Containing PEG-like Sequences to Form Flexible and Degradable Films for Sustainable Packaging. *Polym. Degrad. Stab.* **2019**, *169*, 108963. https://doi.org/10.1016/j.polymdegradstab.2019.108963.

(27)   Guidotti, G.; Soccio, M.; Gazzano, M.; Fusaro, L.; Boccafoschi, F.; Munari, A.; Lotti, N. New Thermoplastic Elastomer Triblock Copolymer of PLLA for Cardiovascular Tissue Engineering: Annealing as Efficient Tool to Tailor the Solid-State Properties. *Polymer (Guildf)*. **2021**, *213*, 123336. https://doi.org/10.1016/j.polymer.2020.123336.

(28)   Flores, I.; Martínez de Ilarduya, A.; Sardon, H.; Müller, A. J.; Muñoz-Guerra, S. ROP and Crystallization Behaviour of Partially Renewable Triblock Aromatic-Aliphatic Copolymers Derived from L-Lactide. *Eur. Polym. J.* **2020**, *122*, 109321. https://doi.org/10.1016/j.eurpolymj.2019.109321.

(29) Jian, J.; Xiangbin, Z.; Xianbo, H. An Overview on Synthesis, Properties and Applications of Poly(Butylene-Adipate-Co-Terephthalate)–PBAT. *Adv. Ind. Eng. Polym. Res.* **2020**, *3* (1), 19–26. https://doi.org/10.1016/j.aiepr.2020.01.001.

(30) Guidotti, G.; Soccio, M.; García-Gutiérrez, M. C.; Ezquerra, T.; Siracusa, V.; Gutiérrez-Fernández, E.; Munari, A.; Lotti, N. Fully Biobased Superpolymers of 2,5-Furandicarboxylic Acid with Different Functional Properties: From Rigid to Flexible, High Performant Packaging Materials. *ACS Sustain. Chem. Eng.* **2020**, *8* (25), 9558–9568. https://doi.org/10.1021/acssuschemeng.0c02840.

(31) Papamokos, G.; Dimitriadis, T.; Bikiaris, D. N.; Papageorgiou, G. Z.; Floudas, G. Chain Conformation, Molecular Dynamics, and Thermal Properties of Poly(n-Methylene 2,5-Furanoates) as a Function of Methylene Unit Sequence Length. *Macromolecules* **2019**, *52*, 6533–6546. https://doi.org/10.1021/acs.macromol.9b01320.

(32) Tsanaktsis, V.; Terzopoulou, Z.; Nerantzaki, M.; Papageorgiou, G. Z.; Bikiaris, D. N. New Poly(Pentylene Furanoate) and Poly(Heptylene Furanoate) Sustainable Polyesters from Diols with Odd Methylene Groups. *Mater. Lett.* **2016**, *178*, 64–67. https://doi.org/10.1016/j.matlet.2016.04.183.

(33) Robles-Hernández, B.; Soccio, M.; Castrillo, I.; Guidotti, G.; Lotti, N.; Alegria, A.; Martínez-Tong, D. E. Poly(Alkylene 2,5-Furanoate)s Thin Films: Morphology, Crystallinity and Nanomechanical Properties. *Polymer (Guildf).* **2020**, *204* (9), 122825. https://doi.org/10.26434/chemrxiv.12309755.v1.

(34) Papageorgiou, G. Z.; Papageorgiou, D. G.; Terzopoulou, Z.; Bikiaris, D. N. Production of Bio-Based 2,5-Furan Dicarboxylate Polyesters: Recent Progress and Critical Aspects in Their Synthesis and Thermal Properties. *Eur. Polym. J.* **2016**, *83*, 202–229. https://doi.org/10.1016/j.eurpolymj.2016.08.004.

(35) Guidotti, G.; Soccio, M.; García-Gutiérrez, M. C.; Gutiérrez-Fernández, E.; Ezquerra, T. A.; Siracusa, V.; Munari, A.; Lotti, N. Evidence of a 2D-Ordered Structure in Biobased Poly(Pentamethylene Furanoate) Responsible for Its Outstanding Barrier and Mechanical Properties. *ACS Sustain. Chem. Eng.* **2019**, *7* (21), 17863–17871. https://doi.org/10.1021/acssuschemeng.9b04407.

(36) Guidotti, G.; Mart, D. E.; Soccio, M.; Robles-Hernandez, B.; Gazzano, M.; Lotti, N.; Alegria, A. Evidence of Nanostructure Development from the Molecular Dynamics of Poly (Pentamethylene 2 , 5-Furanoate). *Macromolecules* **2020**, *53* (23), 10526–10537. https://doi.org/10.1021/acs.macromol.0c02297.

(37) Soccio, M.; Martínez-Tong, D. E.; Guidotti, G.; Robles-Hernández, B.; Munari, A.; Lotti, N.;

Alegria, A. Broadband Dielectric Spectroscopy Study of Biobased Poly(Alkylene 2,5-Furanoate)s' Molecular Dynamics. *Polymers (Basel).* **2020**, *12* (6), 1355. https://doi.org/10.3390/polym12061355.

(38)   Hedenqvist, M. S. *Barrier Packaging Materials*, 2nd ed.; Elsevier, 2012. https://doi.org/10.1016/B978-1-4377-3455-3.00027-4.

(39)   Weinberger, S.; Canadell, J.; Quartinello, F.; Yeniad, B.; Arias, A.; Pellis, A.; Guebitz, G. M. Enzymatic Degradation of Poly(Ethylene 2,5-Furanoate) Powders and Amorphous Films. *Catalysts* **2017**, *7* (11), 318. https://doi.org/10.3390/catal7110318.

(40)   Sonnenschein, M. F. Introduction to Polyurethane Chemistry. In *Polyurethanes: Science, Technology, Markets, and Trends*; John Wiley & Sons, Inc, 2015; pp 105–126. https://doi.org/10.1002/9781118901274.

(41)   Fabbri, M.; Soccio, M.; Costa, M.; Lotti, N.; Gazzano, M.; Siracusa, V.; Gamberini, R.; Rimini, B.; Munari, A.; García-Fernández, L.; Vázquez-Lasa, B.; San Román, J. New Fully Bio-Based PLLA Triblock Copoly(Ester Urethane)s as Potential Candidates for Soft Tissue Engineering. *Polym. Degrad. Stab.* **2016**, *132*, 169–180. https://doi.org/10.1016/j.polymdegradstab.2016.02.024.

(42)   Mensitieri, G.; Di Maio, E.; Buonocore, G. G.; Nedi, I.; Oliviero, M.; Sansone, L.; Iannace, S. Processing and Shelf Life Issues of Selected Food Packaging Materials and Structures from Renewable Resources. *Trends Food Sci. Technol.* **2011**, *22* (2), 72–80. https://doi.org/10.1016/j.tifs.2010.10.001.

(43)   Tokiwa, Y.; Calabia, B. P. Biodegradability and Biodegradation of Polyesters. *J. Polym. Environ.* **2007**, *15* (4), 259–267. https://doi.org/10.1007/s10924-007-0066-3.

(44)   Gigli, M.; Quartinello, F.; Soccio, M.; Pellis, A.; Lotti, N.; Guebitz, G. M.; Licoccia, S.; Munari, A. Enzymatic Hydrolysis of Poly(1,4-Butylene 2,5-Thiophenedicarboxylate) (PBTF) and Poly(1,4-Butylene 2,5-Furandicarboxylate) (PBF) Films: A Comparison of Mechanisms. *Environ. Int.* **2019**, *130*, 104852. https://doi.org/10.1016/j.envint.2019.05.046.

Graphic for Manuscript

1
2
3
4
5
6
7
8
9
10
11
12
13
14
15
16
17
18
19
20
21
22
23
24
25
26
27
28
29
30
31
32
33
34
35
36
37
38
39
40
41
42
43
44
45
46
47
48
49
50
51
52
53
54
55
56
57
58
59
60

1
2
3
4
5
6
7
8
9
10
11
12
13
14
15
16
17
18
19
20
21
22
23
24
25
26
27
28
29
30
31
32
33
34
35
36
37
38
39
40
41
42
43
44
45
46
47
48
49
50
51
52
53
54
55
56
57
58
59
60